

Article

Impacts of Casson Model on Hybrid Nanofluid Flow over a Moving Thin Needle with Dufour and Soret and Thermal Radiation Effects

Vinodh Srinivasa Reddy ¹, Jagan Kandasamy ^{1,*}  and Sivasankaran Sivanandam ² 

¹ Department of Mathematics, School of Engineering, Presidency University, Bangalore 560064, India

² Mathematical Modelling and Applied Computation Research Group, Department of Mathematics, King Abdulaziz University, Jeddah 21589, Saudi Arabia

* Correspondence: kjaganppmaths@gmail.com

Abstract: The current study used a novel Casson model to investigate hybrid Al₂O₃-Cu/Ethylene glycol nanofluid flow over a moving thin needle under MHD, Dufour–Soret effects, and thermal radiation. By utilizing the appropriate transformations, the governing partial differential equations are transformed into ordinary differential equations. The transformed ordinary differential equations are solved analytically using HAM. Furthermore, we discuss velocity profiles, temperature profiles, and concentration profiles for various values of governing parameters. Skin friction coefficient increases by upto 45% as the Casson parameter raised upto 20%, and the heat transfer rate also increases with the inclusion of nanoparticles. Additionally, local skin friction, a local Nusselt number, and a local Sherwood number for many parameters are entangled in this article.

Keywords: hybrid nanofluid; thin needle; Casson model; MHD; thermal radiation; Dufour and Soret effect



Citation: Reddy, V.S.; Kandasamy, J.; Sivanandam, S. Impacts of Casson Model on Hybrid Nanofluid Flow over a Moving Thin Needle with Dufour and Soret and Thermal Radiation Effects. *Math. Comput. Appl.* **2023**, *28*, 2. <https://doi.org/10.3390/mca28010002>

Academic Editor: Zhuojia Fu

Received: 15 November 2022

Revised: 19 December 2022

Accepted: 22 December 2022

Published: 27 December 2022



Copyright: © 2022 by the authors. Licensee MDPI, Basel, Switzerland. This article is an open access article distributed under the terms and conditions of the Creative Commons Attribution (CC BY) license (<https://creativecommons.org/licenses/by/4.0/>).

1. Introduction

Due to their improved ability for heat transmission, nanoliquids are used in a wide variety of industrial applications, such as papermaking, heat exchangers, microelectronic devices, nuclear reactors, geothermal power generation, and transportation, to name only a few examples. The consumption of nanosolutions is less prominent in certain heat transfer applications. Hybrid nanofluids, which combine two different kinds of nanoparticles in regular fluids, are being developed to get around this drawback. The diameter of hybrid or combined nanomaterials, such as nanofluid with a single component or nanoparticle, ranges from 10 to 100 nm. Wang et al. [1] looked into heat transfer in nanofluids, primarily concerned with the preparation of nanofluids, recent experiments, and analytical studies of nanofluids. The same authors, Wang et al. [2], conducted the subsequent discussion of nanofluid applications as well as their flow and heat transfer characteristics in forced and free convection flows. Future research avenues are also implied [3–6], and they contain additional related works. Salleh et al. [7] investigated incompressible flow and wall heat transfer on a delicate, thin needle saturated with an Al₂O₃-Cu/water flow while taking buoyancy effects into account. Kavya et al. [8] looked into the issue of the Williamson hybrid nanofluid in a stretching cylinder with water-based Cu and MoS₄ nanoparticles. The results indicate a decline in the heat transfer properties of the Williamson hybrid nanofluid flow with increasing Prandtl numbers and curvature parameter values. Raju et al. [9–11] investigated the flow and heat transmission characteristics of a nanofluid in a contracting or expanding porous channel with different permeabilities under the influence of MHD and thermal radiation.

Casson fluid is used to characterize non-Newtonian fluid behavior. The applications of non-Newtonian fluids include drag-reducing agents, printing technology, damping and

braking devices, personal protective equipment and food products. Souayeh et al. [12] and Bilal et al. [13] investigated an incompressible non-Newtonian MHD Casson nanoliquid along a thin needle. Ibrar et al.'s [14] investigation into the effects of thermally radiative magneto-nano Casson fluid toward thin needles used the Navier slip effect to model the issue mathematically. Jyothi et al. [15] examined the effects of non-linear thermal radiation on the Casson liquid flow past a moving thin needle. According to the findings, heat transfer is improved by higher values of Brownian motion, thermophoresis, Dufour number, heating, and radiative parameters. The goal of Mamatha et al.'s [16] research was to examine the flow, heat, and mass transport of a hybrid nanofluid Casson and micropolar fluid across a curved stretching sheet. Compared to micropolar and Casson fluids, hybrid nanofluid has a higher temperature profile. The objective of Sulochana et al. [17] was to investigate the Casson/Carreau hybrid nanoliquid boundary layer behavior over an immeasurably poignant needle in the presence of unpredictable heat sources and thermal radiation.

MHD research has been documented in geophysical and astrophysical challenges. Due to its numerous advantages in the engineering, engineering technology, and petroleum refining fields, this topic has attracted a lot of attention recently. Magnetofluid examples include metals, plasma, electrolytes, and salts. The fundamental concept behind MHD is that magnets can disperse moving liquids by absorbing undercurrents, which alter the magnetic force. Raju et al. [18] made an attempt to study the effects of cross-diffusion on the MHD non-linear radiative Carreau fluid over a wedge containing gyro-microorganisms. As a result, both the injection flow case and the suction flow case exhibit high rates of mass and heat transfer. In this article, Mamatha et al. [19] investigated the movement of an electrically conducting, incompressible fluid over a stretching sheet. The thermal boundary layer is managed by the Cattaneo-Christov heat flux theory. Waini et al. [20] found that the local Nusselt number and skin friction coefficient on the needle surface tend toward increasing with decreasing needle size and an increasing volume fraction of copper (Cu) nanoparticles. Sulochana et al. [21] also discussed the exploration of the MHD hybrid nanofluid flow's periphery layer in addition to a horizontally positioned, continuously moving needle. A study by Madhukesh et al. [22] examined the main concept of their study: hybrid nanomaterial liquid flow past a thin needle under convective boundary conditions, magnetic flow, and thermophoretic force. Nurul Amira Zainal et al. [23] aimed to analyze the heat transfer performance of unsteady magnetohydrodynamics in hybrid nanofluids, and a heat generation impact and stability analyses were performed.

A material emits thermal radiation as a result of its heat, and the characteristics of thermal radiation depend on the material's temperature. One of the most crucial process variables for the movement of heat and fluid in high-temperature thermal systems is radiation properties. A non-linear stretching sheet with a convective boundary is used in Jagan et al.'s [24] investigation of how thermal radiation affects the magneto-convection of a micropolar nanoliquid. The rise in the thermal radiation parameter results in higher temperature profiles. Kejela et al. [25] and Nazar et al. [26] have produced additional works in this area. Nurul Amira Zainal et al. [27,28] investigated the unsteady Maxwell hybrid nanofluid toward a stretching or shrinking surface with thermal radiation and heat transfer. Additionally, results shows that the skin friction coefficient increases by nanoparticles and suction parameters. Nurul Amira Zainal et al. [29] studied the flow and heat transfer in the stagnation region employing the Maxwell hybrid nanofluid, and the results were obtained using the Bvp4c technique in the MATLAB platform.

Temperature gradients cause mass flux, known as the Soret (thermal diffusion) effect. The concentration differences that cause energy flux are known as the "diffusion-thermo" (Dufour) effect. Dufour and Soret effects are encountered in many practical applications, such as in the areas of geosciences and chemical engineering. The Tiwari and Das models are employed by Iskandar et al. [30] and Khan et al. [31] to mathematically analyze the flow of (Al_2O_3 -water) nanoliquid and (AA7072-AA7075/water) hybrid nanofluid over a moving thin needle. Additionally, the combined effect of the Dufour and Soret diffusions

tend to increase the heat transfer coefficient; however, the mass transfer coefficient exhibits dual behaviors.

According to the studies mentioned above and through the analysis of a literature survey, a research gap was found regarding hybrid nanofluid flow over a moving thin needle with Dufour and Soret effects using the Casson model. In the current study, a recently developed Casson model was used to discuss the flow of hybrid (Al₂O₃-Cu/Ethylene glycol) nanofluids over a moving thin needle. Additional MHD, thermal radiation, and Dufour and Soret effects are included. The HAM technique in the Mathematica software has been used to solve the specified problem in this study. Furthermore, tables and graphs are used to present the noteworthy physical quantities varying with parameters.

2. Mathematical Formulation of the Problem

Figure 1 illustrates the flow of a hybrid (Al₂O₃-Cu/Ethylene glycol) nanofluid over a lateral moving thin needle with radius $c = 0.1$. In cylindrical coordinates, variables x and r represent axial and radial coordinates, respectively. The thin needle's velocity U_w can move in the same direction or on the opposite direction of the free stream velocity U_∞ . Furthermore, a magnetic field perpendicular to the direction of flow is applied. It is also assumed that the concentrations at the wall and in the area are constant. Furthermore, it is assumed that the fundamental equations contain terms for MHD, thermal radiation, and Soret and Dufour terms.

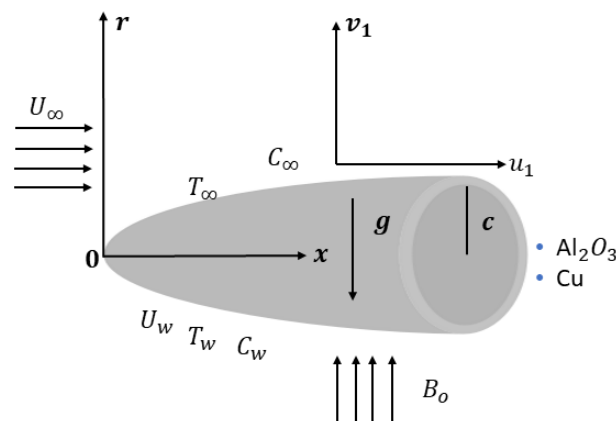


Figure 1. Physical diagram.

The rheological expression of the Casson fluid can be defined as follows (refer to Ibrar et al. [14]):

$$\tau_{ij} = \begin{cases} 2(\mu_B + p_y/\sqrt{2\pi})e_{ij}, & \pi > \pi_c, \\ 2(\mu_B + p_y/\sqrt{2\pi_c})e_{ij}, & \pi < \pi_c, \end{cases}$$

where product value of the non-Newtonian model is expressed as π_c , yield stress of the fluid model is denoted by P_y , π is the deformation rate product component, and viscosity of plastic deformation of the Casson fluid is represented as μ_B .

The radiative linear heat transfer is described in the following Equation (3); therefore, thermal radiation effect is given by:

$$q_r = \frac{4\sigma^*}{3k^*} \frac{\partial T^4}{\partial r}$$

We developed the flow governing equations, which are given below (refer to Mamatha et al. [16], Sulochana et al. [17,21], and Waini et al. [30]):

$$\frac{\partial(ru_1)}{\partial x} + \frac{\partial(rv_1)}{\partial r} = 0 \tag{1}$$

$$u_1 \frac{\partial u_1}{\partial x} + v_1 \frac{\partial u_1}{\partial r} = \frac{\mu_{hmf}}{\rho_{hmf}} \left(1 + \frac{1}{\alpha}\right) \frac{1}{r} \frac{\partial}{\partial r} \left(r \frac{\partial u_1}{\partial r}\right) - \frac{\sigma_{hmf} B_0^2 u_1}{\rho_{hmf}} \tag{2}$$

$$\left. \begin{aligned} u_1 \frac{\partial T}{\partial x} + v_1 \frac{\partial T}{\partial r} &= \frac{k_{hmf}}{(\rho C_p)_{hmf}} \frac{1}{r} \frac{\partial}{\partial r} \left(r \frac{\partial T}{\partial r}\right) + \frac{1}{(\rho C_p)_{hmf}} \frac{\partial(q_r)}{\partial r} \\ &+ \frac{\rho_{hmf}}{(\rho C_p)_{hmf}} \frac{D_m K_T}{C_s} \frac{1}{r} \frac{\partial}{\partial r} \left(r \frac{\partial C}{\partial r}\right) \end{aligned} \right\} \tag{3}$$

$$u_1 \frac{\partial C}{\partial x} + v_1 \frac{\partial C}{\partial r} = \frac{D_m}{r} \frac{\partial}{\partial r} \left(r \frac{\partial C}{\partial r}\right) + \frac{D_m K_T}{T_m} \frac{1}{r} \frac{\partial}{\partial r} \left(r \frac{\partial T}{\partial r}\right) \tag{4}$$

With the associated boundary condition:

$$\left. \begin{aligned} u_1 = U_w, \quad v_1 = 0, \quad T = T_w, \quad C = C_w \text{ at } \eta = c.? \\ u_1 \rightarrow U_\infty, \quad T \rightarrow T_\infty, \quad C \rightarrow C_\infty \text{ as } r \rightarrow \infty \end{aligned} \right\} \tag{5}$$

where u_1 and v_1 represent the x - and r -axis velocity components, respectively, and T is the hybrid nanofluid’s temperature. A list of the physical traits of a base fluid and a nanoparticle and correlations of hybrid nanofluid, respectively, can be found in Tables 1 and 2. ϕ_1 and ϕ_2 stands for volume fraction nanoparticles of Al_2O_3 and Cu, respectively.

Table 1. Thermophysical properties of nanoparticles and base fluid (Sulochana et al. [17]).

Properties	Al_2O_3	Cu	Ethylene Glycol
ρ (kg.m ⁻³)	3970	8933	1190
k (W.m ⁻¹ .K ⁻¹)	40	400	0.258
C_p (J.kg ⁻¹ .K ⁻¹)	765	385	2400
σ (Ω .m ⁻¹)	1.502×10^{-10}	5.96×10^7	10.7×10^{-5}

Table 2. Correlations of hybrid nanofluids (refer to Sulochana et al. [17], Madhukesh et al. [22], and Nurul Amira Zamal et al. [23]).

Properties	Nanofluid	Hybrid Nanofluid
Density	$\rho_{nf} = \phi_1 \rho_{s1} + (1 - \phi_1) \rho_f$	$\rho_{hmf} = [\phi_1 \rho_{s1} + (1 - \phi_2) \rho_f] (1 - \phi_1) + \phi_2 \rho_{s2}$
Heat capacity	$(\rho C_p)_{nf} = (1 - \phi_1) (\rho C_p)_f + \phi_1 (\rho C_p)_{s1}$	$(\rho C_p)_{hmf} = [(1 - \phi_2) (\rho C_p)_f + \phi_1 (\rho C_p)_{s1}] (1 - \phi_1) + \phi_2 (\rho C_p)_{s2}$
Dynamic viscosity	$\mu_{nf} = \frac{\mu_f}{(1 - \phi_1)^{2.5}}$	$\mu_{hmf} = \frac{\mu_f}{(1 - \phi_1)^{2.5} (1 - \phi_2)^{2.5}}$
Thermal conductivity	$\frac{k_{nf}}{k_f} = \frac{k_{s1} - 2\phi_1(k_f - k_{s1}) + 2k_f}{k_{s1} + \phi_1(k_f - k_{s1}) + 2k_f}$	$\frac{k_{hmf}}{k_f} = \frac{k_{s2} + k_{nf}(2 - 2\phi_2) + 2\phi_2 k_{s2}}{k_{s2} - \phi_2 k_{s2} + k_{nf}(2 + \phi_2)}$
Electrical Conductivity	$\frac{\sigma_{nf}}{\sigma_f} = \frac{\sigma_{s1} - 2\phi_1(\sigma_f - \sigma_{s1}) + 2\sigma_f}{\sigma_{s1} + \phi_1(\sigma_f - \sigma_{s1}) + 2\sigma_f}$	$\frac{\sigma_{hmf}}{\sigma_f} = \frac{\sigma_{s2} + \sigma_{nf}(2 - 2\phi_2) + 2\phi_2 \sigma_{s2}}{\sigma_{s2} - \phi_2 \sigma_{s2} + \sigma_{nf}(2 + \phi_2)}$

The appropriate modifications are (refer to Sulochana et al. [17]):

$$\varphi = v_f x f(\eta), \quad \theta(\eta) = \frac{T - T_\infty}{T_w - T_\infty}, \quad \eta = \frac{Ur^2}{v_f x}, \quad \phi(\eta) = \frac{C - C_\infty}{C_w - C_\infty} \tag{6}$$

Using (6) into Equations (2)–(5), they are reduced as follows:

$$\frac{2}{B_1 B_2} \left(1 + \frac{1}{\alpha}\right) (\eta f''' + f'') + f f'' - \frac{X_1}{B_2} M f' = 0 \tag{7}$$

$$\frac{2}{Pr C_2} (C_1 + 4/3 * Rd) (\theta' + \eta \theta'') + f \theta' + 2Du(\phi' + \eta \phi'') = 0 \tag{8}$$

$$\frac{2}{Sc}(\phi' + \eta\phi'') + f\phi' + 2Sr(\theta' + \eta\theta'') = 0 \tag{9}$$

subjected to:

$$\left. \begin{aligned} f(c) &= \frac{\varepsilon}{2} * c, f'(c) = \frac{1}{2} * \varepsilon, \theta(c) = 1, \phi(c) = 1 \text{ at } \eta = c \\ f'(\eta) &= \frac{1}{2} * (1 - \varepsilon), \phi(\eta) \rightarrow 0, \theta(\eta) \rightarrow 0 \text{ as } \eta \rightarrow \infty \end{aligned} \right\} \tag{10}$$

where $B_1 = \frac{\mu_f}{\mu_{hmf}}, B_2 = \frac{\rho_{hmf}}{\rho_f}, B_3 = \frac{\sigma_{hmf}}{\sigma_f}, B_4 = \frac{k_{hmf}}{k_f}$ and $B_5 = \frac{(\rho C_p)_{hmf}}{(\rho C_p)_f}$ are the constants. $\nu_f = \frac{\mu_f}{\rho_f}, \varepsilon = \frac{U_w}{U}, Pr = \frac{(\mu C_p)_f}{k_f}, M = \frac{\sigma_f B_0^2 x}{2u\rho_f}, Du = \frac{D_m K_T (C_w - C_\infty)}{C_s \nu_f (C_p)_f (T_w - T_\infty)}, Rd = \frac{4\sigma^* T_\infty^3}{K^* K_f}, Sr = \frac{D_m K_T (T_w - T_\infty)}{T_m \nu_f (C_w - C_\infty)}, Sc = \frac{\nu_f}{D_m}$, and $Re_x = \left(\frac{Ux}{\nu_f}\right)$ represent the Prandtl number, kinematic viscosity, velocity ratio parameter, magnetic parameter, Dufour–Soret parameters, thermal radiation, Schmidt number, and Reynolds number, respectively.

Equation (11) defines the skin friction coefficient (C_f), Nusselt number (Nu_x), and Sherwood number (Sh_x) (refer to Iskandar Waini et al. [30]):

$$C_f = \frac{2\tau_w}{\rho_f U^2}, Nu_x = \frac{xq_w}{k_f(T_w - T_\infty)} \text{ and } Sh_x = \frac{xq_m}{D_m(C_w - C_\infty)} \tag{11}$$

where shear stress, heat flux, and mass flux are defined as (refer to Iskandar Waini et al. [30]):

$$\tau_w = \mu_{hmf} \left(1 + \frac{1}{\alpha}\right) \left(\frac{\partial u}{\partial r}\right)_{r=R(x)}, q_w = \left(-k_{hmf} \frac{\partial T}{\partial r} + q_r\right)_{r=R(x)} \text{ and } q_m = -D_m \left(\frac{\partial C}{\partial r}\right)_{r=R(x)} \tag{12}$$

Using Equations (6) and (11) in Equation (12), the following equations are obtained:

$$C_f(Re_x)^{1/2} = \frac{4c^{1/2}}{B_1} \left(1 + \frac{1}{\alpha}\right) f''(c) \tag{13}$$

$$Nu_x(Re_x)^{-1/2} = -2c^{1/2} \left(C_1 + \frac{4}{3}Rd\right) \theta'(c) \tag{14}$$

$$Sh_x(Re_x)^{-1/2} = -2c^{1/2} \phi'(c) \tag{15}$$

3. Method of Solution

The resulting Equations (7)–(9) with boundary conditions (10), chosen as initial guesses and auxiliary linear operators, are then solved by HAM (refer to Hayat et al. [4] and Jagan et al. [24]):

$$\begin{aligned} f_0(\eta) &= \frac{\varepsilon}{2} * \eta + \left(\frac{1}{2} - \varepsilon\right) * (\eta - c + \exp(c - \eta)) \\ \theta_0(\eta) &= \exp(c - \eta), \phi_0(\eta) = \exp(c - \eta) \\ L_f(f) &= \frac{\partial^3 f}{\partial \eta^3} - \frac{\partial f}{\partial \eta}, L_\theta(\theta) = \frac{\partial^2 \theta}{\partial \eta^2} - \theta, L_\phi(\phi) = \frac{\partial^2 \phi}{\partial \eta^2} - \phi \end{aligned}$$

which satisfies the property:

$$L_f[H_1 + H_2 * \exp(\eta) + H_3 * \exp(-\eta)] = 0 \tag{16}$$

$$L_\theta[H_4 * \exp(\eta) + H_5 * \exp(-\eta)] = 0 \tag{17}$$

$$L_\phi[H_6 * \exp(\eta) + H_7 * \exp(-\eta)] = 0 \tag{18}$$

where H_1, H_2, \dots, H_7 are arbitrary constants.

Figure 2 illustrates how the auxiliary parameters h_f, h_θ , and h_ϕ , which are included in the HAM solution, influence how quickly the HAM solutions converge. Plotting of the h-curve for the following values: $\phi_1 = 0.01, \phi_2 = 0.01, \varepsilon = 1, \alpha = 1, Pr = 7, Sr = 0.1, c = 0.1$,

$M = 0.1, Rd = Du = 0.2,$ and $Sc = 0.6.$ Figure 2 clearly shows that the permitted range of curves is $-0.3 \leq h_f \leq 0.1, -0.29 \leq h_\theta \leq 0.05,$ and $-0.31 \leq h_\phi \leq 0.05.$ Convergence of the profiles is tabulated in Table 3.

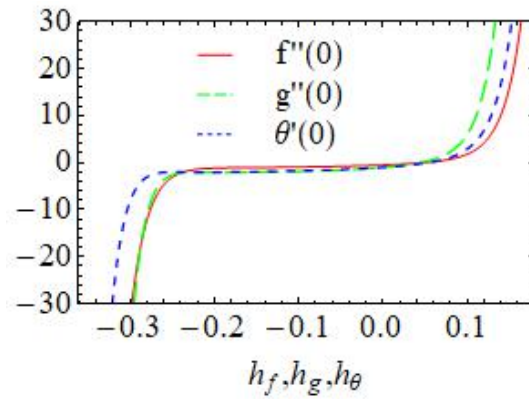


Figure 2. The h -curves of $h_f, h_\theta,$ and $h_\phi.$

Table 3. Convergences of series $\phi_1 = 0.01, \phi_2 = 0.01, \epsilon = 1, \alpha = 1, Pr = 7, Sr = 0.1, c = M = 0.1, Rd = Du = 0.2,$ and $Sc = 0.6.$

Order	$-f''(c)$	$-\theta'(c)$	$-\phi'(c)$
1	0.50000	1.00001	1.00001
5	0.50002	1.00005	1.00004
10	0.50004	1.00011	1.00008
15	0.50006	1.00015	1.00012
20	0.50009	1.0002	1.00016
25	0.50011	1.00025	1.0002
30	0.50013	1.0003	1.00024
35	0.50016	1.00035	1.00029
40	0.50018	1.0004	1.00033

4. Results and Discussions

HAM is an analytic approximation method to solve highly nonlinear problems. By using this method, the highly nonlinear and coupled Equations (7)–(9) and the corresponding boundary Equation (10) are solved. The discussions are set up to address various combinations of relevant study-related factors. The variation of $\alpha, M, Du, Rd,$ and Sr is shown in Figures 3–5. From Figures 6–9 displays the variation of $\alpha, M, Du,$ and $Rd.$ Table 4 displays the computed values of $\alpha, M, Du,$ and Rd for $C_f(Re_x)^{0.5}, Nu_x(Re_x)^{-0.5},$ and $Sh_x(Re_x)^{-0.5}.$

Figure 3a,b, shows the profile of velocity reduces as α and M rises. Physically, increasing the Casson parameter causes an enhancement in the fluid’s dynamic viscosity, which reduces fluid motion and results in a decrease in the profile of velocity. Additionally, by increasing $M,$ the velocity profile decreases, because magnetic fields produce Lorentz forces that oppose motion.

Figure 4a,b displays the profile of temperature rises as Du and Rd rise. Enlarging the value of Du is thought to improve the temperature profile. “ Du ” is a technical term that describes how a concentration gradient affects the flow of thermal energy flux. Rd also compares the importance of thermal radiation dominant over a conduction heat transfer. As the radiation parameter is increased, the temperature within the boundary layer naturally increases.

Table 4. $C_f(Re_x)^{0.5}$, $Nu_x(Re_x)^{-0.5}$, and $Sh_x(Re_x)^{-0.5}$ number values computed for various physical parameters.

α	M	Du	Rd	$C_f(Re_x)^{0.5}$	$Nu_x(Re_x)^{-0.5}$	$Sh_x(Re_x)^{-0.5}$
1	0.1	0.2	0.2	-2.30857	-1.92005	-1.75259
1.4				-1.63701	1.46098	1.46092
1.7				1.46086	1.04996	1.04996
2				1.04991	1.04987	1.04983
1	0.1	0.2	0.2	-2.30857	-2.37217	-2.43422
	0.2			-2.4948	1.46113	1.46059
	0.3			1.46006	1.45955	1.05001
	0.4			1.0496	1.0492	1.04881
1	0.1	0.2	0.1	-2.30857	-2.30857	-2.30857
			0.2	-2.30857	1.17214	1.46113
			0.3	1.71912	1.9514	1.0528
			0.4	1.05001	1.04792	1.04628
1	0.1	0.1	0.2	-2.30857	-2.30857	-2.30857
		0.2		-2.30857	1.44608	1.46113
		0.3		1.4762	1.49127	1.05029
		0.4		1.05001	1.04974	1.04946

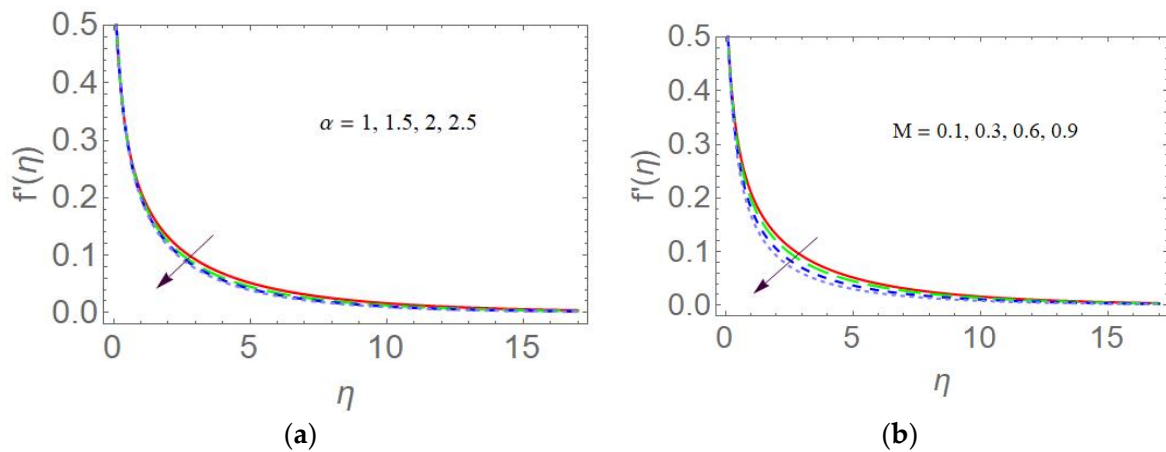


Figure 3. Impacts of (a) Casson parameter α on $f'(\eta)$ and (b) Magnetic parameter M on $f'(\eta)$.

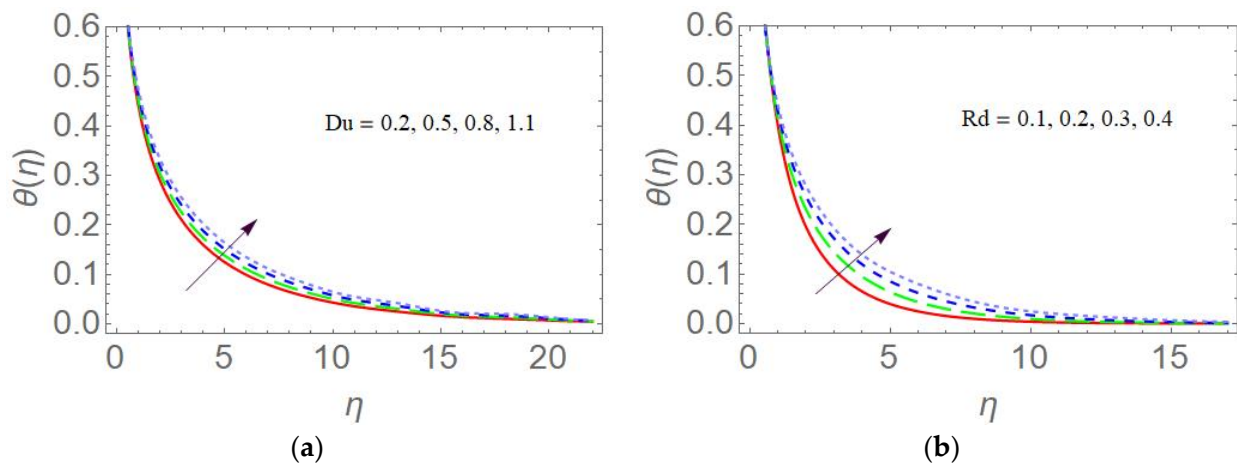


Figure 4. Impacts of (a) Dufour parameter Du on $\theta(\eta)$ and (b) Radiation parameter Rd on $\theta(\eta)$.

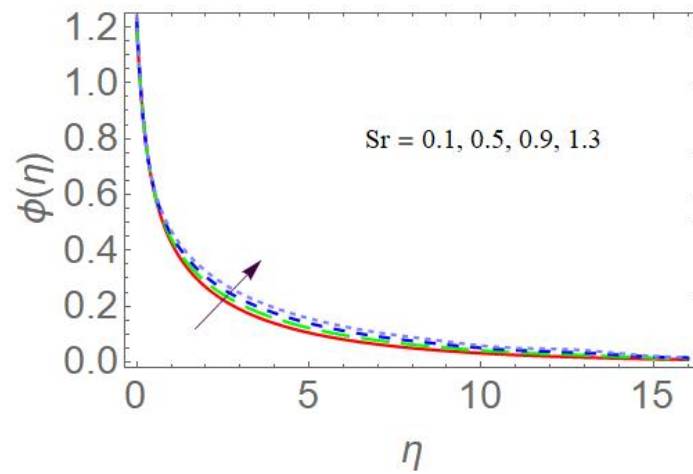
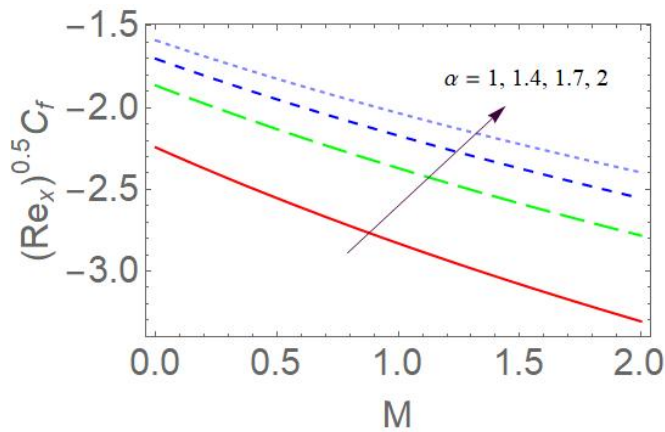
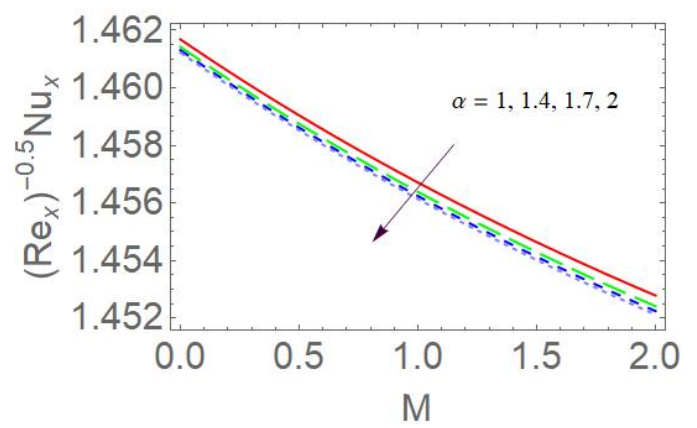


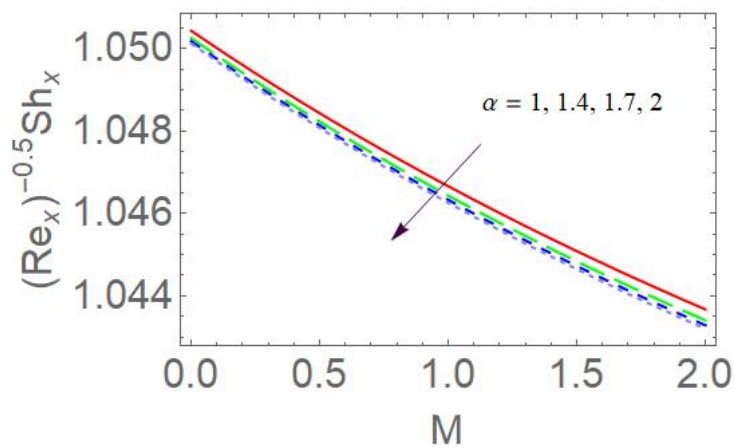
Figure 5. Impacts of Sr on $\phi(\eta)$.



(a)



(b)



(c)

Figure 6. Influence of (a) α on $C_f(Re_x)^{0.5}$, (b) α on $Nu_x(Re_x)^{-0.5}$, and (c) α on $Sh_x(Re_x)^{-0.5}$.

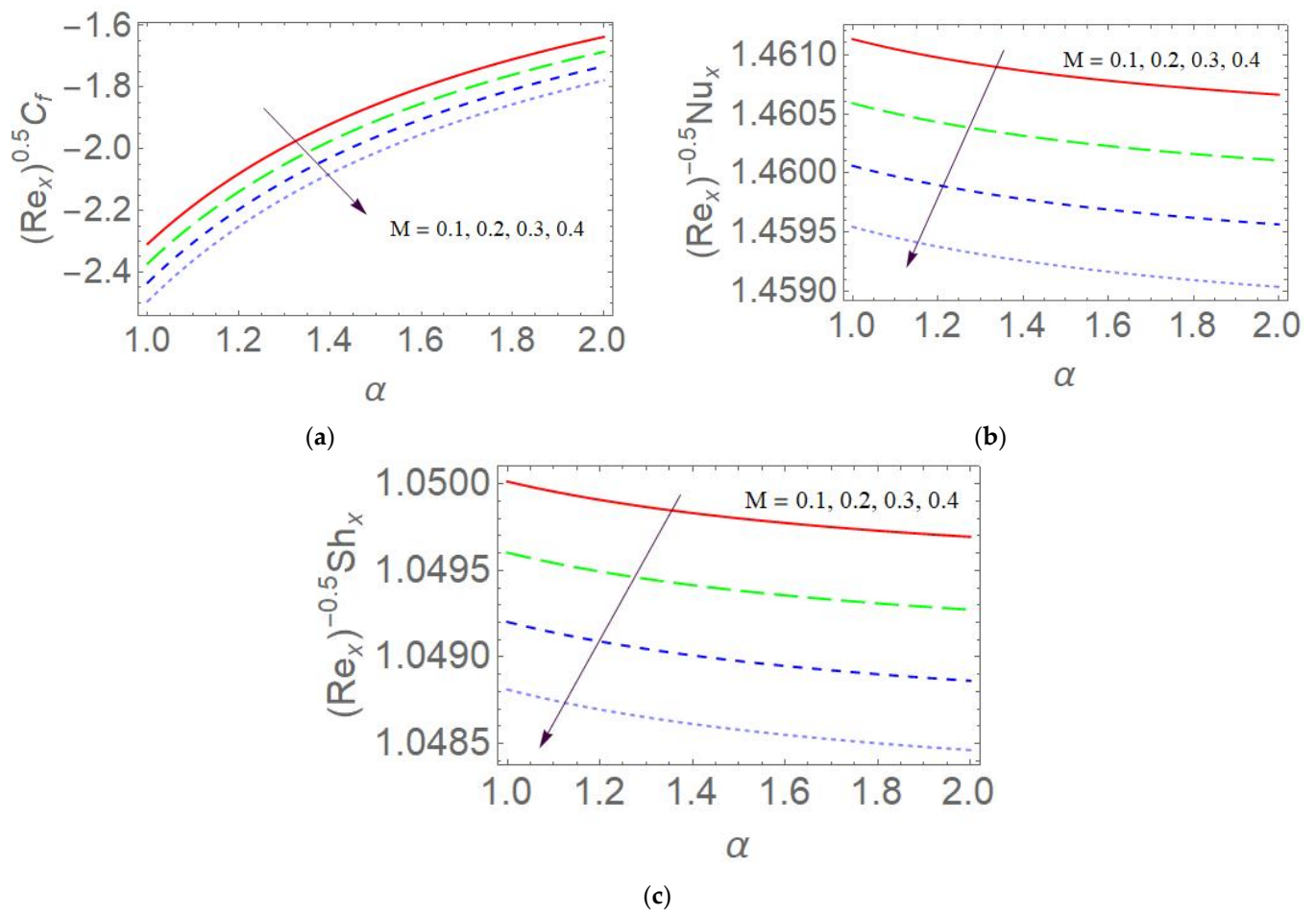


Figure 7. Influence of (a) M on $C_f(Re_x)^{0.5}$, (b) M on $Nu_x(Re_x)^{-0.5}$, and (c) M on $Sh_x(Re_x)^{-0.5}$.

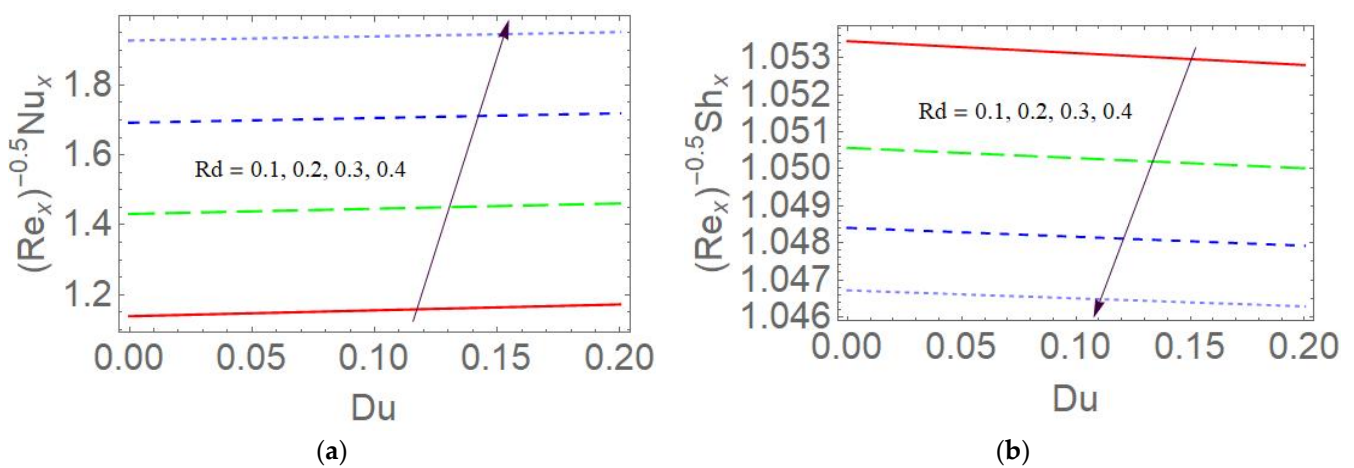


Figure 8. Impacts of (a) Rd on $Nu_x(Re_x)^{-0.5}$ and (b) Rd on $Sh_x(Re_x)^{-0.5}$.

Figure 5 displays the profile of concentration for various Sr values. The figure shows how increasing the Sr increases the concentration profile. Soret is a temperature gradient effect on concentration distribution. Physically, higher Soret numbers correspond to a greater temperature gradient, resulting in greater convective flow. As a result, the concentration distribution improves.

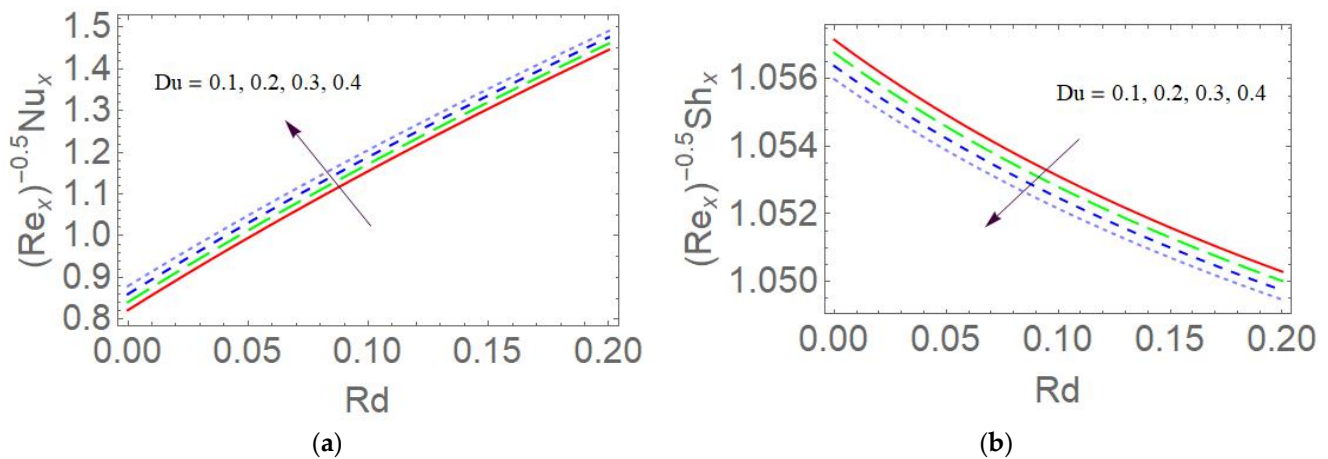


Figure 9. Impacts of (a) Du on $Nu_x(Re_x)^{-0.5}$ and (b) Du on $Sh_x(Re_x)^{-0.5}$.

As shown in Figure 6a–c, increasing the value of α causes C_f to increase, but Nu_x and Sh_x decreases sharply. As shown in Figure 7a–c, when the magnetic parameter increases, the C_f , Nu_x , and Sh_x numbers decrease sharply, because magnetic fields produce Lorentz forces that oppose motion due to drag force between the fluid and the surface. The impact of Rd on the Nu_x and Sh_x is shown in the Figure 8a,b. Increasing the non-linear thermal radiation, the thickness of the boundary layer increases, which results in a decrease in the heat transfer rate, whereas mass transfer rate decreases. The effect of Du on the Nu_x and Sh_x is depicted in Figure 9a,b. The Nu_x is increased and the Sh_x is decreased by increasing the Du .

5. Conclusions

The Casson model was used to investigate the impact of the Dufour and Soret effects, thermal radiation, and magnetic field on hybrid nanofluid flow over a thin needle.

- The boundary layer that forms around the needle is equally tiny in size.
- The series solution is obtained with the proposed HAM method. HAM gives better approximations than other numerical methods.
- In total, 2% nanoparticles are included and the rate of heat transfer increases up to 45%.
- The Casson parameter tends to makes the flow field smaller. Physically, increasing the Casson parameter causes an enhancement in the fluids dynamic viscosity, which reduces the fluid motion and results in a decrease in the profile of velocity.
- As the magnetic field strength increases, the velocity profiles become narrower, because magnetic fields produce Lorentz forces that oppose motion.
- As a result of the thermal radiation being included, heat is transferred more quickly.
- As the radiation parameter is increased, the temperature within the boundary layer naturally increases, because thermal radiation is dominant over a thermal conduction heat transfer.
- The rates of mass and heat transfer as well as the Dufour and Soret effects are accelerated, because with the Dufour effect, the concentration gradient affects the flow of thermal energy flux, and higher Soret numbers correspond to a greater temperature gradient, resulting in a greater convective flow.
- The present results are useful in the cooling technology and thermal science community.

Author Contributions: Conceptualization, J.K. and S.S.; methodology, J.K.; software, J.K. and V.S.R.; validation J.K.; formal analysis, J.K., S.S. and V.S.R.; investigation, J.K.; resources, J.K.; writing—original draft preparation, J.K. and V.S.R.; writing—review and editing, J.K.; visualization, J.K.; supervision, J.K. All authors have read and agreed to the published version of the manuscript.

Funding: This research received no external funding.

Data Availability Statement: Not applicable.

Conflicts of Interest: The authors declare no conflict of interest.

Abbreviations

In this document, the following abbreviations are used.

<i>MHD</i>	Magneto hydrodynamics
<i>HAM</i>	Homotopy Analysis Method
<i>c</i>	needle radius (m)
U_w	velocity at the surface ($\text{m}\cdot\text{s}^{-1}$)
C_w	wall concentration
T_w	temperature at the surface (K)
C_∞	ambient concentration
T_m	temperature of mass fluid (K)
K^*	coefficient of mean absorption ($\text{c}\cdot\text{m}^{-1}$)
C_s	concentration susceptibility
U_∞	free stream velocity ($\text{m}\cdot\text{s}^{-1}$)
C_p	specific heat ($\text{kg}^{-1}\cdot\text{J}$)
D_m	mass diffusion coefficient ($\text{m}^2\cdot\text{s}^{-1}$)
T_∞	ambient temperature (K)
u_1, v_1	velocity components along x and r directions ($\text{m}\cdot\text{s}^{-1}$)
q_r	radiative heat flux ($\text{kg}\cdot\text{m}^2\cdot\text{s}^{-3}$)
K_T	ratio of thermal diffusion
C_f	Skin friction
Sh_x	Sherwood number
C	fluid concentration
Nu_x	Nusselt number

Greek symbols

ν	kinematic viscosity ($\text{m}^2\cdot\text{s}^{-1}$)
α	Casson parameter
ρ	fluid density ($\text{kg}\cdot\text{m}^{-3}$)
ε	velocity ratio parameter
μ	dynamic viscosity of a fluid ($\text{m}^2\cdot\text{s}^{-1}$)
σ^*	Stefan-Boltzmann constant ($\text{W}\cdot\text{m}^{-2}\cdot\text{K}^{-4}$)

Subscripts

<i>hnf</i>	hybrid nanofluid
'	differentiation w.r.t. η
<i>nf</i>	nanofluid
<i>f</i>	fluid
∞	ambient

References

1. Wang, X.Q.; Mujumdar, A.S. A review on nanofluids—Part I: Theoretical and numerical investigations. *Braz. J. Chem. Eng.* **2008**, *25*, 613–630. [[CrossRef](#)]
2. Wang, X.Q.; Mujumdar, A.S. A review on nanofluids—Part II: Experiments and applications. *Braz. J. Chem. Eng.* **2008**, *25*, 631–648. [[CrossRef](#)]
3. Kamyar, A.; Saidur, R.; Hasanuzzaman, M. Application of Computational Fluid Dynamics (CFD) for nanofluids. *Int. J. Heat Mass Transf.* **2012**, *55*, 4104–4115. [[CrossRef](#)]
4. Hayat, T.; Sabir Ali, S.; Qasim, M.; Asghar, S. Three-dimensional stretched flow via convective boundary condition and heat generation/absorption. *Int. J. Numer. Methods Heat Fluid Flow* **2012**, *24*, 342–358. [[CrossRef](#)]
5. Sidik, N.A.C.; Adamu, I.M.; Jamil, M.M.; Kefayati, G.H.R.; Mamat, R.; Najafi, G. Recent progress on hybrid nanofluids in heat transfer applications: A comprehensive review. *Int. Commun. Heat Mass Transf.* **2016**, *78*, 68–79. [[CrossRef](#)]
6. Rostami, M.N.; Dinarvand, S.; Pop, I. Dual solutions for mixed convective stagnation-point flow of an aqueous silica–alumina hybrid nanofluid. *Chin. J. Phys.* **2018**, *56*, 2465–2478. [[CrossRef](#)]
7. Alwani, S.S.N.; Norfifah, B.; Norihan, A.; Fadzilah, A. Effect of Buoyancy force on the flow and heat transfer around the thin needle in Hybrid nanofluid. *CFD Lett.* **2020**, *12*, 22–36.

8. Kavva, S.; Nagendramma, V.; Ameer Ahammad, N.; Sohail, A.; Raju, C.S.K. Magnetic-hybrid nanoparticles with stretching/shrinking cylinder in a suspension of MoS₄ and copper nanoparticles. *Int. Comm. Heat Mass Transf.* **2022**, *136*, 106150. [[CrossRef](#)]
9. Raju, C.S.K.; Ameer Ahammad, N.; Kiran, S.; Nehad Ali, S.; Se-Jin, Y.; Dinesh Kumar, M. Nonlinear movements of axisymmetric ternary hybrid nanofluids in a thermally radiated expanded or contracting permeable Darcy walls with different shapes and densities: Simple linear aggression. *Int. Comm. Heat Mass Transf.* **2022**, *135*, 106110. [[CrossRef](#)]
10. Priyadarshini, P.; Vanitha Archana, N.; Ameer Ahammad, N.; Raju, C.S.K.; Se-Jin, Y.; Nehad Ali, S. Gradient descent machine learning regression for MHD flow: Metallurgy process. *Int. Comm. Heat Mass Transf.* **2022**, *138*, 106307. [[CrossRef](#)]
11. Hu Ge, J.; Nehad Ali, S.; Mahrous, Y.M.; Pooja, S.; Raju, C.S.K.; Mamatha Upadhya, S. Radiated magnetic flow in a suspension of ferrous nanoparticles over a cone with Brownian motion and thermophoresis. *Case Stud. Therm. Eng.* **2021**, *25*, 100915.
12. Basma, S.; Reddy, M.G.; Sreenivasulu, P.; Poornima, T.; Rahimi, G.M.; Alarifi, M.I. Comparative analysis on non-linear radiative heat transfer MHD Casson nanofluid past a thin needle. *J. Mol. Liq.* **2019**, *284*, 163–174.
13. Bilal, M.; Urva, Y. Analysis of non-Newtonian fluid flow over a fine rotating thin needle for variable viscosity and activation energy. *SN Appl. Sci.* **2020**, *2*, 677. [[CrossRef](#)]
14. Ibrar, N.; Reddy, M.G.; Shehzad, S.A.; Sreenivasulu, P.; Poornima, T. Interaction of single and multi -walls carbon nanotubes in magnetized- nano Casson fluid over radiated horizontal needle. *SN Appl. Sci.* **2020**, *2*, 677. [[CrossRef](#)]
15. Jyothi, A.M.; Naveen Kumar, R.; Punith Gowda, R.J.; Prasanna kumara, B.C. Significance of Stefan blowing effect on flow and heat transfer of Casson nanofluid over a moving thin needle. *Commun. Theor. Phys.* **2021**, *73*, 0253–6102. [[CrossRef](#)]
16. Mamatha Upadhya, S.; Shiva Rama Raju, S.V.; Raju, C.S.K.; Nehad Ali, S.; Jae Dong, C. Importance of entropy generation on Casson, Micropolar and Hybrid magneto-nanofluids in a suspension of cross section. *Chin. J. Phys.* **2021**, *77*, 1080–1101. [[CrossRef](#)]
17. Sulochana, C.; Poornima, M.; Sandeep, N.; Gangadhar, P.A.K. Effect of variable heat generation/absorption on magnetohydrodynamic Sakiadis flow of Casson/Carreau hybrid nano liquid due to a persistently moving needle. *Heat Transfer* **2021**, *50*, 8354–8377.
18. Raju, C.S.K.; Ibrahim, S.K.; Anuradha, S.; Priyadarshini, P. Bio-convection on non-linear radiative flow of a Carreau fluid over a moving wedge with suction or injection. *Eur. Phy. J. Plus* **2016**, *131*, 409. [[CrossRef](#)]
19. Upadhya, S.M.; Mahesha; Raju, C.S.K. Cattaneo-Christov heat flux model for magnetohydrodynamic flow in a suspension of dust particles towards a stretching sheet. *Nonlinear Eng.* **2018**, *3*, 237–246. [[CrossRef](#)]
20. Iskandar, W.; Anuar, I.; Pop, I. Hybrid nanofluid flow and heat transfer past a vertical thin needle with prescribed surface heat flux. *Int. J. Numer. Methods Heat Fluid Flow* **2019**, *29*, 4875–4894.
21. Sulochana, C.; Aparna, S.R.; Sandeep, N. Impact of linear/nonlinear radiation on incessantly moving thin needle in MHD quiescent Al-Cu/methanol hybrid nanofluid. *Int. Ambient. Energy* **2020**, *43*, 2694–2700. [[CrossRef](#)]
22. Madhukesh, K.; Ramesh, G.K.; Alsulami, M.D.; Prasanna kumara, B.C. Characteristic of thermophoretic effect and convective boundary thermal conditions on flow of hybrid nanofluid over a moving thin needle. In *Waves in Random and Complex Media*; Taylor & Francis: Abingdon, UK, 2021. [[CrossRef](#)]
23. Zainal, N.A.; Roslinda, N.; Kohilvani, N.; Pop, I. Stability analysis of unsteady MHD Rear stagnation point flow of hybrid nanofluid. *Mathematics* **2021**, *9*, 2428. [[CrossRef](#)]
24. Jagan, K.; Sivasankaran, S.; Bhuvaneswari, M.; Rajan, S. Effect of Thermal Radiation on Magneto-Convection of a Micropolar Nano liquid towards a Non-Linear Stretching Surface with Convective Boundary. *Int. J. Eng. Technol.* **2018**, *7*, 417–421. [[CrossRef](#)]
25. Solomon, B.K.; Mitiku, D.; Abebe, G. Investigation of Effects of Thermal Radiation, Magnetic Field, Eckert Number and Thermal Slip on MHD Hiemenz Flow by Optimal Homotopy Asymptotic Method. *J. Math.* **2021**, *2021*, 5590657. [[CrossRef](#)]
26. Zainal, N.A.; Roslinda, N.; Kohilvani, N.; Pop, I. Unsteady flow of a Maxwell hybrid nanofluid past a stretching/shrinking surface with thermal radiation effect. *Appl. Math. Mech.* **2021**, *42*, 1511–1524. [[CrossRef](#)]
27. Zainal, N.A.; Roslinda, N.; Kohilvani, N.; Pop, I. Unsteady stagnation point flow past a permeable stretching/shrinking rigid plate in Al₂O₃-Cu/water hybrid nanofluid with thermal radiation. *Int. J. Numer. Methods Heat Fluid Flow* **2021**, *32*, 2640–2658. [[CrossRef](#)]
28. Zainal, N.A.; Roslinda, N.; Kohilvani, N.; Ioan Pop, I. The impact of thermal radiation on Maxwell hybrid nanofluids in the stagnation point. *Nanomaterials* **2022**, *12*, 1109. [[CrossRef](#)]
29. Tayyaba, N.; Bhatti, M.M.; Efstathios Michaelides, E. Hybrid (Au-TiO₂) nanofluid flow over a thin needle with magnetic field and thermal radiation: Dual solutions and stability analysis. *Microfluid. Nano Fluid.* **2022**, *26*, 2. [[CrossRef](#)]
30. Iskandar, W.; Anuar, I.; Pop, I. Dufour and Soret effects on Al₂O₃-water nanofluid flow over a moving thin needle: Tiwari and Das model. *Int. J. Numer. Methods Heat Fluid Flow* **2020**, *31*, 766–782. [[CrossRef](#)]
31. Umair, K.; Zaib, A.; Sakhinah Abu, B.; Anuar, I. Forced convection flow of water conveying AA7072 and AA7075 alloys-nanomaterials on variable thickness object experiencing Dufour and Soret effects. *Sci. Rep.* **2022**, *12*, 6940.

Disclaimer/Publisher's Note: The statements, opinions and data contained in all publications are solely those of the individual author(s) and contributor(s) and not of MDPI and/or the editor(s). MDPI and/or the editor(s) disclaim responsibility for any injury to people or property resulting from any ideas, methods, instructions or products referred to in the content.